University of Nevada, Reno

Altered Basalts from Hawaii as an Analog for Alteration on Mars

A thesis submitted in partial fulfillment
of the requirements for the degree of

Bachelor of Science in Geophysics and the Honors Program

by

Brandon Rasmussen

Dr. Wendy Calvin, Thesis Advisor

August, 2017

UNIVERSITY OF NEVADA RENO

THE HONORS PROGRAM

We recommend that the thesis
prepared under our supervision by

Brandon Rasmussen

entitled

Altered Basalts from Hawaii as an Analog for Alteration on Mars

be accepted in partial fulfillment of the
requirements for the degree of

BACHELOR OF SCIENCE, GEOPHYSICS

_____

Wendy Calvin, Ph.D., Thesis Advisor

_____

Tamara Valentine, Ph. D., Director, **Honors Program**

August, 2017

Abstract

Mars has been a focus of planetary academic research for decades due to relatively new data from spacecraft. Spectral data from both satellite and rover instrumentation have provided identification of a variety of materials. Satellite data have guided future mission plans and deployments by providing coarsely defined areas of interest for up close observation. Recently, spectral data acquired by the Compact Reconnaissance Imaging Spectrometer for Mars (CRISM) on the Mars Reconnaissance Orbiter (MRO) have identified hydrated silicates, carbonates, and serpentines in multiple locations. All of these minerals provide evidence for occurrence of specific surface and crustal processes, many of which can produce habitable environments for simple life. Similar alteration minerals are present in basalt flows from Hawaii in a similar background lithology and present a prime analog for in-depth laboratory study to understand the processes resulting in alteration on Mars.

Reflectance spectroscopy can identify minerals by quantifying how light of various wavelengths reflects from mineral crystals. Alteration minerals are generated from secondary processes after a rock forms, and many have particularly distinctive spectral signatures in the visible to short-wave infrared (VIS-SWIR) wavelengths. Past spectral work has already shown significant evidence of the presence of aqueous activity and associated alteration on Mars (Bibring et al., 2006: Milliken et al., 2008: Ehlmann et al, 2009: Ehlmann, Mustard, & Murchie, 2010). Less defined, however, is the genetic source of these alteration minerals. Finding out whether these minerals formed simply as a past product of surface water interaction with exposed basalt, or represent outcrops of alteration due to groundwater or subsurface water-rock

interactions offers answers to significant scientific questions related to the planet. Also of interest is past (or possibly present) serpentinization, which (when active) produces magnetite and H_2, a possible energy source for aqueous microbial life (Ehlmann, Mustard, & Murchie, 2010). Being able to identify and differentiate between these materials from orbit helps significantly in planning rover traverse paths and in situ targets which can provide more direct verification of mineralogy and lithology.

The first goal of this project is to characterize and identify the genetic origin of alteration products from a unique set of samples extracted from a core hole penetrating deep into the shield volcano Mauna Kea on Hawaii. This project then aims to produce a highly verified library of reflectance spectra representing alteration minerals and mineral assemblages of interest in Mars exploration, with reference to their hypothesized environment and conditions of formation. Several minerals of interest to Mars exploration are identified in bulk reflectance spectra, high resolution reflectance spectra, and through scanning electron microscope (SEM) use.

This work has been successful in creating a quantified library of alteration products found in the Hawaii core. The occurrence and distribution of these mineral classes and mineral combinations have been mapped using sums of reflectance spectra. Several alteration classes of phyllosilicates and zeolites are identified. These classes are mapped in both bulk spectra of the drill core over 3000’ of the field collection and at high spatial resolution in cut sections taken to represent common alteration products. Further refinement of mineral groups to single mineral species requires crystallography information and more quantitative elemental analysis. Future work could identify more specific alteration conditions and apply the library to Mars data.

Acknowledgements

I'd like to thank Wendy Calvin and Joel DesOrmeau, as this project would simply not have been possible without them. Wendy provided constant input and was always available to chat about mapping methodology, theoretical mathematics, and all of the other background knowledge required to develop this piece of work. Joel was not even my project mentor and dedicated hours to helping me with scanning electron microscopy and sample preparation.

I'm humbled to have been funded on three separate projects while working with Wendy, all of which contributed to my ability to complete this thesis. The HURA Award, the NSF-EPSCOR scholarship, and the Goldwater Scholarship combined with departmental funding made all of my research goals, culminating in this thesis, possible.

I would also like to thank all of my geoscience, math, and physics professors at the University of Nevada, Reno whose courses inspired hypotheses and ideas related to spectroscopy and SEM imaging which greatly benefited both myself and this project.

Finally, I'd like to thank the Honors program for presenting me with the opportunity to develop this piece of work, and for guidance throughout my undergraduate career.

Table of Contents

List of Tables:

List of Figures:

Introduction

Spectroscopy on Mars:

Reflectance and transmission spectroscopy has been used as a means to identify geologic materials since the 1950's. However, reflectance spectroscopy in the context of mineral and rock identification at the VIS-SWIR wavelengths was not widely used until the 1970s to the early 1990s. Confidence in the method's ability to determine mineralogy and differentiate between similar minerals was solidified in this period, with comprehensive libraries establishing links between spectral absorption features and mineral composition. The first scanning electron microscopes (SEMs) were developed in the 1950s and 1960s and were immediately recognized for their ability to identify microstructure and morphology of natural materials.

While reflectance spectroscopy has been used as a tool from both satellite and land-based missions on Mars, scanning electron microscopes have only recently been proposed as possible instrumentation for use on Mars (Gaskin, Jerman, Gregory, & Sampson, 2012). This is due to the sensitive nature of the instrumentation, extensive sample preparation, and varying levels of vacuum that an SEM requires (Gotze & Kempe, 2008). Both of these tools have been used to examine key areas on Earth that are identified as analogs to Mars through spectroscopy and geochemistry, mostly in the low to medium-sulfidation epithermal (active geothermal) setting. While spectroscopy provides keys to direct mineralogy, backscattering analysis and imagery of the SEM allow for analyzing morphology, crystal structure, and elemental composition (Calvin & Pace, 2016: Gotze & Kempe, 2008: Shedd, Verta, & Wylie, 1982).

Initial satellite-mounted spectrometers utilizing the infrared wavelengths (much longer than VIS-SWIR) have been in use on Mars in various forms since the 1970s. Earlier efforts were multi-channel, extremely coarse spatial resolution instruments which allowed for inference of bulk rock, ice, and atmosphere composition. These early-era instruments culminated with the Mars Global Surveyor's Thermal Emission Spectrometer (TES) in 1996. Modern spectroscopy relevant to the wavelength range being studied in this paper began via the Observatoire pour la Mineralogie, l'Eau, les Glaces et l'Activité (OMEGA) instrument aboard the Mars Express satellite, though earlier instruments on the Mariner 6 and 7 spacecraft also investigated similar wavelengths.

The Mars Express OMEGA Instrument, which arrived in 2003 (and is still active today), uses the visible through infrared wavelengths at a sufficient (7-13 nanometer) spectral and spatial resolution to identify minerals. It was the first instrument to derive convincing evidence of the widespread distribution of hydrated alteration minerals and sulfates, as well as to differentiate between bulk primary mineral phases (Bibring et al., 2006). Several papers used its coarsely spatially resolved data (~200m to over 1000m sized pixels) to build a narrative of possible Mars history indicated by the distribution of mineral phases. Jean-Pierre Bibring and the OMEGA Team provided a broad overview of the mapped mineralogy, as well as the implications that global mineral distribution has for Mars' atmospheric and crustal evolution (Bibring et al. 2006). The team recognized that the formation of sulfates likely came later in the planets' history, as acidic surface or near surface water created by volcanic outgassing, combined with a fluctuating water table, deposited both evaporate and alteration sulfate phases (gypsum, jarosite, alunite, etc.) (Bibring et al., 2006). They also recognized the broad distribution of Fe-rich hydrated phyllosilicates (clays) and the broad, blanket-like covering of much of the planet due to ferric

oxide-dominated dust. However, due to the coarse spatial resolution, fine features in the VIS-SWIR which help to indicate genetic sources of hydrated phyllosilicates could not be resolved. The paper only discusses possible environments of formation, mainly hinting at subsurface formation by discussion of stratigraphic constraints such as dominant outcrops being exposed in craters, and erosional surfaces (Bibring et al., 2006). These broader identifications, along with older TES publications, led to much more focused Mars analog studies on Earth in the early 2000's in locations such as Iceland, California, South America, the Western United States and Hawaii (Ming et al. 2003: Ehlmann, Bish, Ruff, & Mustard, 2012: McCanta, Dyer, & Triedman, 2014)

With the Compact Reconnaissance Imaging Spectrometer for Mars (CRISM) instrument aboard the Mars Reconnaissance Orbiter (MRO), spatial resolution was improved from kilometer or more sized pixels, to 18 meters. This resolution allows for interpretations of single-outcrop sized areas and for more robust inspection of lower-concentration minerals. Multiple, more recent papers by the CRISM team and their collaborators have begun to target smaller areas of Mars and identify its heterogeneity, which is much more significant than originally thought. Aqueous phases have now been studied in several different distinct zones on Mars, and genetic alteration sources have been theorized to range from impact and shock generated material to low-temperature metamorphism or hydrothermal activity, to neutral-pH groundwater interaction (Milliken et al., 2008: Ehlmann et al, 2009: Ehlmann, Mustard, & Murchie, 2010: Tornabene et al., 2013). For the most part, significant surficial geomorphic features, which could be linked to large bodies of water or Earth-like rivers, are old and inferred to have occurred during a very early wet-period on Mars (inferred to be > 3.5 Ga), though recent studies show a possible Earth-like, wet environment much more recently (slightly over 2.5 billion years ago) at mid-latitudes

(Wilson, Howard, Moore, & Grant, 2016). All of these possibilities carry with them distinct stratigraphic constraints, mineralogy, and morphologies which can be studied in greater detail on Earth.

Some minerals of interest on Mars which allow for correlation to specific genetic sources of aqueous/upper crustal processes are hydrated silicates (zeolites, clays, etc.), sulfates, prehnite, multiple oxide phases, anhydrous phyllosilicates (micas like chlorite, serpentine, and muscovite-sericite), and amorphous silica (hydrated and anhydrous) (Milliken et al., 2008: Ehlmann et al, 2009: Ehlmann, Mustard, & Murchie, 2010: Tornabene et al., 2013). These phases, combined with morphologies, and elemental partitioning, represent specific chemistries, as well as temperature-pressure-pH conditions which can be tied to unique genetic sources. The core being studied in this project is from the shield and post-shield phase of the Mauna Kea volcano, and though it is billions of years younger than most outcropped basalt on Mars, it contains very similar mineralogy to many regions characterized by the CRISM team on Mars, such as Nili Fossae. The first identifications of analcime (a zeolite) and serpentine on Mars were made at Nili Fossae in 2009 (Ehlmann et al., 2009). Initial analysis of the core shows that analcime is present in our samples, making the samples highly relevant as a Mars analog.

Hawaii Drill Core:

The Humu'ula Groundwater Research Project (HGRP) drilled a continuously-cored hole in the saddle region of the Big Island of Hawaii in March of 2013. The goal of the project was to identify ground water and geothermal energy resources. A series of perched aquifers were identified at local ambient temperatures, but these aquifers were underlain by a regional water table showing considerably higher temperatures that increased with depth. PTA-1, the core

surveyed for this study, started at an elevation of 6385 feet (1946 m) and drilled 5786 feet (1764m) to reach an elevation of 182m above sea level. The core traverses various sub-aerial lava flows, representing both the shield-building phase of the island and the post-shield phase. Figure 1 below illustrates imagery acquired as part of core logging, which was performed for all of the recovered core.

Figure 1: One box of typical core from the HGRP project. The white minerals here are zeolites, while the black and brown minerals are different pyroxenes. The green minerals towards the top of the second column from the left are olivine crystals. Morphological features like the banding and vesicle abundance were logged by colleagues at the University of Hawaii, and interpretations are available online at: https://www.higp.hawaii.edu/hggrc/projects/humuula-groundwater-research-project/hgrp-data/.

The lithology is dominantly basalt with varying amounts of plagioclase and olivine phenocrysts. Both pahoehoe and a'a textures are identified as well as some explosive units, scoria, ash, glass and a few sedimentary units. Logging of PTA-1 noted that discontinuous alteration became prevalent starting at ~ 1km depth. In May of 2014, visible and infrared spectra were collected from the lower half of the PTA-1 core from depths of 3190' to 5785' (972 to 1763 m). Based on preliminary analysis of this data, twenty-five cut sections were acquired, representing the spectral diversity of the sampled core. Eight samples representing the range of alteration were measured using a prototype micro-imaging spectrometer, the Ultra-Compact Imaging Spectrometer (UCIS), and SEM. Though the drilling project was not planned as a Mars analog study, the host lithology, alteration products observed, and alteration conditions provide a unique and highly relevant terrestrial analog to Mars.

Mauna Kea as a Mars Analog and Samples Used in this Study:

The basalts of Mauna Kea have been studied as Mars analogs, but almost exclusively in samples from the near surface, including high-sulfidation acid-sulfate type zones. Several studies have tied Hawaiian samples, both spectrally and geochemically, to several areas on Mars (Ming et al. 2003: McCanta, Dyer, & Triedman, 2014). Lithology within the drill core is almost exclusively young basalt flows (only small strips of possible soil horizons, explosive units, and diamictites interrupt the basalt), which are mostly calcic plagioclase and pyroxene rich, with many flows containing abundant olivine as well. Mars at the near surface, as shown by multiple landed missions, is almost entirely composed of very similar lithology.

Due to its high peak, combined with variable topography and multiple locations covered in rock slides, Mauna Kea has proved to be an effective location for testing of instrumentation

designed for the Moon and Mars. Multiple studies in the past decade have taken advantage of the remote yet accessible location to test instrumentation in missions designed to emulate Mars rover traversal missions (Blumers, Hamilton, Sanders, Zacny, Caillibot, Craft . . . Sellar, 2013 & Graham, Morris, Graff, Yingst, Kate, Glavin . . . Mumm, 2013). In addition to the similar composition of study targets, the location provides traversal challenges similar to those presented in true landed missions with uneven terrain. The UCIS instrument used in our study was designed and proposed by Jet Propulsion Laboratory as an instrument suited for rover implementation on Mars, so data presented later in this paper referring to cut-slabs can be thought of as an analog to data that could be acquired by future Mars missions.

Where this project varies significantly from past studies of Mauna Kea is with the use of samples that have not been exposed to the current surface weathering environment, and the use of very high spatial resolution VIS-SWIR spectroscopy. Also novel is the direct correlation of VIS-SWIR spectra with SEM imaging. These samples have not been previously examined and represent a newly uncovered genetic origin of low-temperature groundwater alteration only accessible and vertically preserved due to core drilling to over 5000’ depths. Although the Mauna Kea samples being studied are much younger than exposed rocks on Mars, surface weathering occurs at an exponentially lower rate on Mars due to differing atmospheric and surface conditions, so that ancient alteration products are still preserved on the present Martian surface.

Completed work will generate a greater understanding of stratigraphic constraints of a Mars analog system. In this case, the intent of the collection of samples was actually to search for groundwater to supply the remote Pohakuloa Training Area with local, potable water. It just so happens that this location is also a great analog for Mars. Because of the unique dataset,

combined with SEM and high resolution UCIS spectroscopy (only available from JPL), this project will provide a unique insight into the depth-component of a low-temperature aqueous Mars analog available in very few other locations on Earth.

Genetic Origin Differentiation and Notes on Alteration:

Although there is diversity within the composition of the bulk rock mass composing most of the core, alteration minerals within each lithologic type are still strongly tied to the conditions at which they formed. As an example, olivine is a common primary mafic mineral formed at high temperatures and present in nearly all of the unaltered portions of the samples collected. Olivine is an iron or magnesium rich silicate and is unstable at atmospheric conditions or near-surface conditions, readily altering to more stable phases. However, a single olivine crystal of identical composition could alter to dozens of different products depending on pressure and temperature conditions, fluid interaction and that fluid's composition, availability of elements from surrounding material, and pH conditions. In addition to alteration mineral elemental compositions, specific textures, morphologies, and structures all provide clues to genetic origins of specific alteration products. Many of these characteristics are directly observable with scanning electron microscopy.

A Mg-rich olivine in a higher-temperature (300 C), CO_2 and Cl^- fluid-rich environment (a very likely composition for near-surface hydrothermal temperature fluids in Hawaii) readily alters to serpentines, carbonates like magnesite and dolomite, and brucite (Ueda, Sawaki, & Maruyama, 2017). This same olivine crystal at a lower temperature can also alter into many of the same products. However, indicator products like certain chlorites and epidote only form at higher temperature, and thus, can indicate higher temperature alteration. Hydrothermal-type illite

clays only form at temperatures higher than those present at the surface. Using these indicator minerals and tying them to associated zeolite composition might aid in observing temperature zonation (Triana, Herrera, Rios, Castellanos, Henao, Williams, & Roberts, 2012).

Also of interest in differentiating between surface alteration and subsurface alteration are biogenic textures. If freshly extruded basalt is exposed to surface processes, alteration minerals rapidly begin to form. In addition, chemical reactions produce H_2, and oxygen and water are available, so conditions for microbial life become ideal. As alteration products are generated, microbial life often leaves signatures within forming mineral textures such as anomalous "microspheres", where cells previously existed and new material grew around them. These spheres (often only 1-4 micrometers across) are often well-preserved and visible in surface-formed zeolites with high magnification imaging. These spheres also would generally have an anomalously high carbon concentrations, though this is difficult to determine with carbon-coated SEM samples like those used in our study. (Pedersen., McLoughlin, Vullum, & Thorseth, 2015).

This project combines high resolution reflectance spectroscopy data with bulk spectroscopy and SEM imaging in order to characterize the nature of alteration in this unique set of Mars analog samples.

Methods

Spectral Collection:

Initial bulk spectra were collected on the HGRP drill core in the field in Hawaii in 2015. Over seven hundred individual bulk spectra were collected using a 7-10 nm resolution Analytical Spectral Device (ASD) field spectrometer. The spectrometer uses two separate detectors to form a single reflectance spectrum composed of wavelengths from 350 to 2500 nanometers (0.35-2.5 μm) a wavelength range commonly used for identifying alteration mineralogy due to hydrated and phyllosilicate minerals' generally high absorption activity in this range (Calvin & Pace, 2016: Clark, 1990).

The spectra were collected by researchers from University of Nevada, Reno using a bare-fiber setup with a controlled light source using a contact probe with a field of view of ~2cm and interfaced with a laptop for in-field quality control and preliminary observation. Measurements were made targeting alteration areas and were not evenly spaced vertically within the core. Notes were taken regarding the depth of each measurement, as well as any significant observations. These bulk spectra were organized into the images shown in Figure 11 as a virtual "stack" of spectra, where each line is a single reflectance spectrum. Using initial spectra combined with visual observation, specific zones of different alteration types were identified and twenty-five small cut-slabs were collected for further lab analysis.

The collected cut-slabs were then measured for their bulk spectra with the ASD and eight samples were selected for measurement at Jet Propulsion Laboratory (JPL) with UCIS. The instrument measured the slab face at an 80 micrometer pixel size in the same wavelength range

as the ASD, allowing for observation of spectra as mostly single minerals. In a few cases, both sides of the cut sample or two pieces of the same sample were imaged, resulting in twelve images of cut faces total. Eight of these twelve UCIS images were analyzed and correlated with SEM images.

Spectral Processing:

The initial bulk spectra were analyzed and decomposed into different endmembers using several methods. Visual observation, spectral angle mapping, linear spectral unmixing, and decorrelation stretching were used on virtual "images" of the core stack where individual pixels represented reflectance spectra. These techniques are described in more detail below. These initial unmixed endmembers were then studied to identify likely constituents of the different alteration zones.

Initial mineral mapping of the cut faces was accomplished using preprocessing and filtering of data in Python before analysis in the ENVI software system. Because pixels are, in most cases, composed of one to two minerals, simple spectral angle mapping (SAM) using spectra from within the image allows for mapping at very high resolution. These images used multiple "endmembers", or representative mineral spectra, from within the image in lieu of pure lab spectra. This analysis, along with all of the analysis and processing not performed in Python, was accomplished using the ENVI software package.

Because of the extremely high spatial resolution, and short scan time, the spectral signal-to-noise level is low, limiting mineral matches due to noise. In order to eliminate this random

noise, all data were processed in Python using a 5-N, 2nd order Savitzky-Golay filter. This filter uses a frequency domain approach to approximate a sort of "sliding" 2nd order polynomial fit across each reflectance spectrum. In general, the filter increases accuracy of mapping broader features in noisy data, but must be done carefully so as to not "over-smooth" the spectra and remove important absorption and reflectance features (Ruffin & King, 1999).

This smoothing method proved to be too drastic for some mapping (see Figure 2 below), so unsmoothed data were used in refined mapping and adjacent pixels were averaged to reduce noise instead. By adding together spectra, random fluctuations in the spectra, which are not actually tied to mineralogy, are suppressed as the variations are added together. Multiple mathematical methods were used to match endmembers to other reflectance spectra. See Figure 2 for a comparison of spectral profiles that highlights the differences between noise suppression methods.

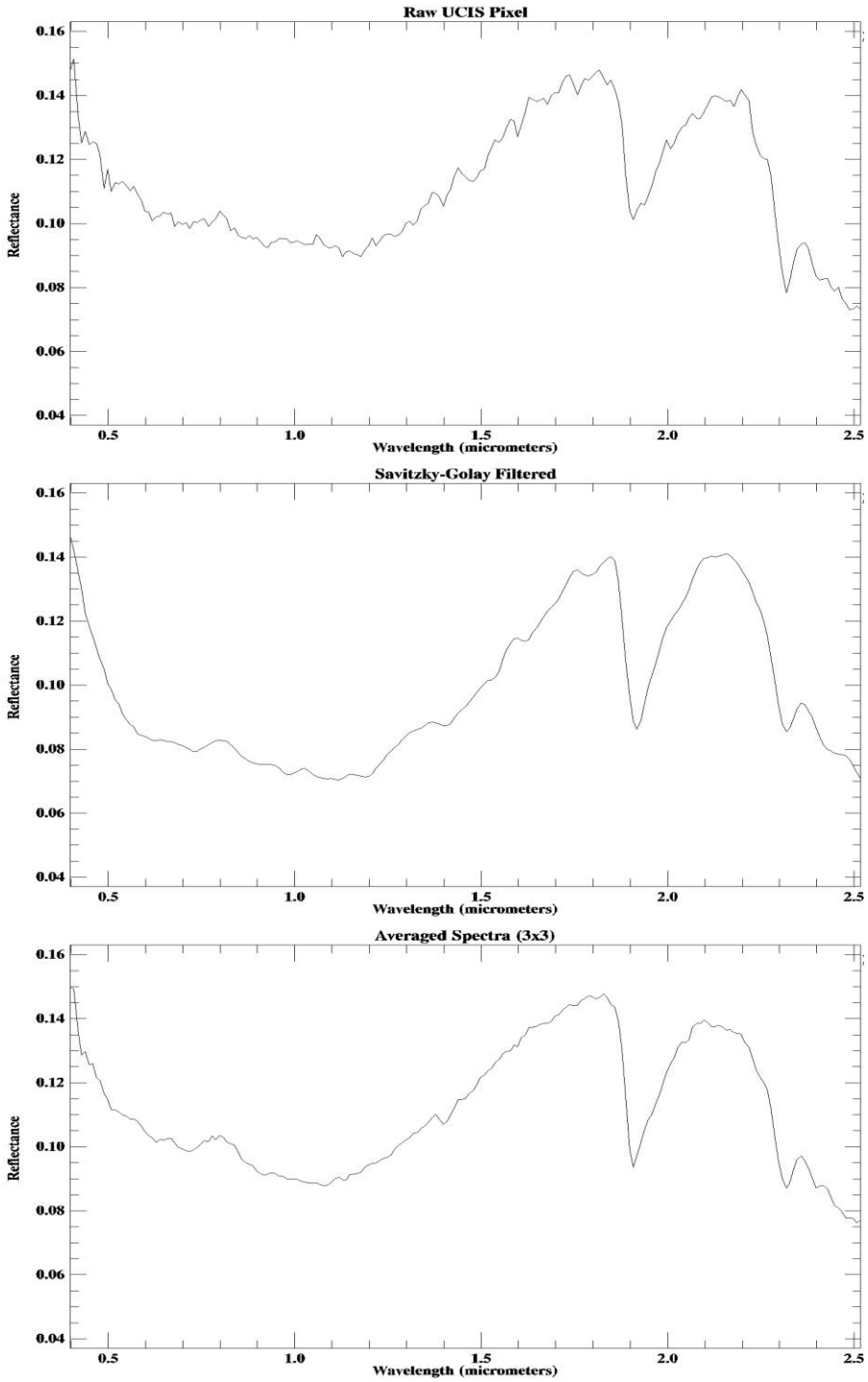

Figure 2: Above are three representations of the same point in a UCIS image. The top plot is extracted from a raw UCIS image, while the other two have been smoothed through the processes outlined in the text. The Savitzky-Golay filter results in the smoothest spectrum, but removes the 2.4 nanometer absorption and introduces artifacts in the lower wavelengths. It also alters the shape of the larger absorptions, which can cause false mapping in spectral feature fitting and linear unmixing. The bottom spectrum is the average of a 3x3 window surrounding the pixel. It maintains spectral shape, while reducing noise and enhancing weaker, real features like the 2.4 micrometer absorption. It sacrifices spatial resolution for cancellation of noise and was found to be superior to filtering in almost all circumstances. The filtered data was adequate for zeolite mapping.

The spectral angle mapping method represents each spectrum as a vector and calculates the angle between each pixel of the image (a single 213 band reflectance spectrum) and a reference spectrum, making matches based upon a set angle allowance. This translates to higher angle values for larger differences in the shape of reflectance spectra at specified wavelengths. SAM is useful when mapping non-mixed spectra but generally weaker in mapping of bulk spectra due to large changes when mineral spectra mix in varying proportions (Kruse, Lefkoff, Boardman, Heidebrecht, Shapiro, Barloon, & Goetz, 1993).

Spectral feature fitting uses a least-squares type approximation to directly measure the difference between a single feature (or a small subset of features) within one reflectance spectrum and target pixels. It calculates the root-mean-squared (RMS) error of the fit, as well as a “scale” indicating a quantification of the match. The overall fit can also be measured as the scale divided by the RMS value, often producing very large numbers for low RMS values. However, histogram stretching of the single-band image (the single band is simply the value of the fit) allows for examination and setting of a custom threshold with which to assign a certain endmember to each pixel (Kruse et al., 1993).

Linear spectral unmixing, used for bulk spectra mapping, is a matrix inverse method. A system of equations is generated from a matrix inverse problem which attempts to rebuild the target pixels with weighted averages of chosen endmembers. Higher weights of specific endmembers generally means that more of the material is present in the pixel. Again, RMS values are generated. In this case, RMS values indicate both if the spectrum was matched well, and whether endmembers are missing (indicated by a large RMS) (Kruse, et al. 1993). Mixing of

mineral spectra is not purely linear physically, but linear unmixing provides a very reasonable estimate of endmember abundances if endmembers are chosen properly and RMS is kept low.

Decorrelation stretching, which was used to identify general variability of the water band for SEM targeting, is another matrix method. It transforms an image of reflectance spectra into a three band RGB (red-green-blue) image, with each band defined by the user. Stretching "around" the 1.91 μm feature requires selection of bands at the edges of a typical water absorption, around 1.85 for blue, 1.91 for green, and 1.97 for red. This produces an image in which relative changes in the values at these wavelengths produce distinctive colors within images and allow a qualitative expression of spectral diversity around this feature (Alley, 1996).

Scanning Electron Microscopy:

Initially, we planned to use two SEMs to map composition of the cut-face samples. These two instruments were the JEOL JSM-6010LA SEM (6010LA) and the JSM-7100FT FESEM (7100T). The 6010LA is a versatile SEM which requires a weaker vacuum than the 7100T, but comes with a less stable and weaker electron beam. This leads to more uncertainty in quantifying elemental composition. The 7100T requires very high vacuum. Due to the vesicular nature of basalt and the abundance of air and water within many samples, the cut-faces needed to have their volume reduced in order to prevent escaping of gas within the vacuum chamber. After the steps outlined below, each sample was mounted to a thin section slide and stabilized on its exterior with epoxy before being cut to roughly 1-1.5mm thicknesses in anticipation of using the 7100T. Even this thickness resulted in too much outgassing, so the 7100T was only used to examine the phyllosilicates in SR-459a. In order to use the 7100T, SR-459a needed to be

fractured to very small pieces, resulting in sample loss and more difficulty in correlating between SEM and UCIS images.

Energy-dispersive X-ray spectroscopy (EDS) was the SEM analysis technique used for determination of elemental composition mapping. EDS essentially bombards a sample with an electron beam, exciting ground-state inner electrons of an element and causing them to be ejected. When outer-shell electrons rush in to fill this unstable configuration, the energy required to make the transition might be ejected as an X-ray. The frequency of this X-ray wave is dependent on its energy, and its energy is dependent on the difference in orbital energies which caused the ejection. These orbital energy differences are well-known and tied to different elements. By observing the energy of these X-rays being ejected from the material over a short time, elements can be identified (Russ, 1984).

EDS requires an extremely clean, flat surface of the sample, as topography will cause scattering of the electron beam and incorrect readings of the ejected X-rays (Russ, 1984). Aqueous alteration generally leads to weaker, less stable material. In the case of this project, several cut-face samples were heavily altered to the point where over 50% of the rock body had been completely altered. Sample preparation for work with the Scanning Electron Microscope (SEM) was uniquely challenging and presented many problems due to both lithology and alteration abundance. After experimentation with several samples, an ideal workflow for preservation of faces to correlate the SEM data with the spectroscopy was developed. The cut-slabs were lightly trimmed by saw to thin-section mount size before a consistent polishing routine was applied to all eight cut-face samples.

Samples were coarsely polished with two different grains of silica-carbide solutions before a series of three different grains of diamond polish were applied by hand with even

pressure. Sonic bathing and rinsing between each phase cleared off ablated material, but was kept to a minimum due to the sonic bath and water's ability to damage fragile alteration minerals like zeolites and clays.

These samples were then carbon coated and analyzed on the low-vacuum JEOL JSM-6010LA SEM. Slabs were examined on the SEM for textures and morphology at magnifications ranging from 39x to 6800x (resulting in scales on the order of one micron). Targets for the SEM were identified through the UCIS imagery by decorrelation stretching around the 1.91 μm water feature, which both visually represented variation in the absorption and identified hydrated alteration minerals versus anhydrous primary minerals. Elemental compositional mapping through EDS was performed using a multiple-pass, mid-range dwell-time method which enhanced signal and reduced noise. EDS analyses were performed at a lower magnification (50x to 190x) and focused mainly on identifying rough cation abundances within alteration products in order to aid in mineral identification.

After analyzing samples within the lower resolution SEM and picking 459a as an ideal target for higher resolution mapping, it was carefully fractured to smaller sized pieces that would not inhibit reaching high-vacuum levels. The 7100-FESEM was then used to observe variation within single vesicle or "vug" infills of alteration products. More advanced mapping software and a much more powerful and stable beam allowed for better estimations of elemental abundances. These better quantifications of elemental abundances helped resolve ambiguity in the spectral mineral interpretations, particularly when trying to differentiate between phyllosilicates.

Despite careful sample preparation, scratches from disintegrating rock chunks during polishing and topography within the samples were unavoidable, and thus, scratch marks and

charging problems can be observed within the images. However, nearly the entire range of alteration diversity noted from the UCIS data was observed on sections of samples which were well-polished and scratch free.

Using notes on texture observations combined with group-averaged zones of EDS data, alteration products were identified for the full range of diversity noted from initial spectral mapping. Zeolites and clays which could not be separated through their stoichiometric ratios and morphologies were either identified through the UCIS spectroscopy (analcime, illite vs smectite-group, etc.) or grouped together (i.e natrolite-like zeolites).

Refined Mapping:

After SEM imaging, it was clear that some endmembers were redundant and that particular features were more important. This led to a revisiting of mineralogy mapping of both UCIS and bulk spectral data. The identified alteration products and groups were noted and representative lab spectra were extracted from the United States Geological Survey archive (Clark, Swayze, Gallagher, King, & Calvin, 1993). After resampling the lab spectra to the same wavelength discretization as the UCIS spectra, spectral angle mapping was performed using the lab spectra as reference spectra.

In order to reduce noise, the images were spatially averaged by a factor of 3, and mapping was performed on these reduced resolution images. Unlike in the initial spectral angle mapping, where a single angle allowance was applied to all images and the endmembers were not allowed to vary, specific endmembers for each image were picked and mapped, with different allowances and wavelength-mapping ranges used to specifically target areas of the spectra most characteristic of specific minerals (generally the 1.8-2.41 micrometer region).

Due to an abnormally large 1.91 micrometer water absorption in many of the phyllosilicate spectra, spectral angle mapping proved to be a poor method for differentiating between zeolites and phyllosilicates. Spectral feature fitting, a least squares fitting of individual absorption features on continuum-removed spectra, was used in its place. Band-thresholding of linearly unmixed bulk spectra was also used, in the case of the ASD collected data. Both of these methods resulted in good fits only when the 2.31 micrometer magnesium vibrational stretch absorption was present, making it useful for differentiation between phyllosilicates and zeolites.

Zeolite spectra from the slabs, while more typical and similar to library spectra, were also generally poorly mapped with spectral angle mapping due to their spectral similarity to each other. Natrolite-group zeolites with extremely broad water absorptions due to complex structure were well mapped with spectral angle mapping due to their uniqueness, but the other potassium and sodium rich zeolites with sharper absorptions also required spectral feature fitting to effectively map. Through these refinements, spatial association of zeolite types became clearer.

In a few cases, mineral mapping was done visually due to information gained from the SEM. Mapping based on experience was also performed on some of the core stack, in order to eliminate clearly anomalous results. This is not an unusual occurrence, as false positives through these statistical and matrix methods are relatively common, particularly when working with noisy data.

Results

Alteration Mineralogy in Cut Slabs:

All eight cut-slabs were examined with both UCIS spectroscopy and SEM imaging, but only 8 of the 12 UCIS images are discussed in this project. The four additional images showed redundant mineralogy to accompanying slabs. Over all eight slabs, six major alteration minerals were found. Four zeolites and two different magnesium-rich phyllosilicates were uniquely identified. The depth at which each sample was collected is shown in Table 1.

SR-392, collected closer to the top of the core hole, was void of alteration minerals. SEM imaging allowed for compositional mapping of the fresh primary minerals which made up the slab. Large phenocrysts of fresh olivine and smaller, though still euhedral and crystalline, clino-pyroxenes made up the majority of the slab with abundant fine-grained calcic plagioclase feldspar. Some large pyroxene phenocrysts were lower in calcium and might represent orthopyroxene, though further study would be needed to confirm this. Olivine crystals were magnesium rich (roughly 25% weight percentage on average), making them more similar to forsterite in composition. This is typical of Hawaiian basalts. Pyroxenes were calcium rich, with both iron and magnesium also present. The matrix also contained ilmenite and, importantly, lacked considerable magnetite and sodium abundance. With all of these characteristics taken into consideration, the basalt can be identified as a typical tholeiitic composition. This alone means that all slabs (which were collected deeper than SR-392) are likely from shield-stage lava flows a little over 250,000 years old, rather than younger alkali-rich post-shield phase lavas. However, this does not mean that all flows in the core are identical in composition. The spectra of all

mapped primary minerals are shown in in Figure 3. These shield phase lavas are not exposed on the surface (Wolfe et al., 1997), and thus, have not been extensively studied in the past with alteration in mind.

Sample ID	Core Scan #	Core Box	Depth (ft)
SR 392	439	805	3386.9
SR 425	533	838	3691.5
SR 459	630	870	3989.1
SR 503	758	915	4417.3
SR 513	187	926	4524.6
SR 537	282	951	4763.4
SR 560	346	976	4991.7
SR 618	33	1036	5573.1

Table 1: A reference table for the depth at which each sample was collected. The core scan number is a unique identifier which allowed for stacking the collected bulk spectra by depth, as shown in Figure 11.

Because the basalts from all of the slabs collected deeper than 392 are likely of a roughly similar starting composition, the prevalence of magnesium rich phyllosilicates is not surprising. Iron was present in significant enough amounts to create characteristic absorptions even in bulk spectra from associated iron-magnesium phyllosilicates. SR-425 was collected only a couple of hundred feet below SR-392, and represented a transitional zone where fresh olivine was still present, but phyllosilicates had formed from olivine crystals. Though both SR-392 and SR-425 are vesicular, empty vesicles are void of alteration minerals. This can be observed in Figure 5 in the true color images. All phyllosilicates in SR-425 are spatially associated with what seem like large crystals of olivine, and represent a spectral endmember with a strong 2.31 micrometer (μm) magnesium-hydroxyl absorption and a weaker 2.4 micrometer absorption. This endmember (saponite) is discussed further below and is shown in Figure 4, which follows the discussion of slab mineralogy.

SR-459a (3989 foot depth) is also representative of phyllosilicate alteration, with the dominant phyllosilicate being the spectral type lacking the 2.25 micrometer iron feature, as in SR 425. This phyllosilicate was identified as saponite due to its swelling texture being indicative of the smectite group (see Figure 7), the large 1.91-μm water band, and an elemental composition of high magnesium with considerable iron. Its color varies significantly across multiple slabs and even within 459a alone, and it may be a mixture of magnesium and iron smectites, a common occurrence in altered basalts. Its composition is consistent, as well as its spectral expression, which consists of a large 1.91-μm water band, a suppressed 1.4-μm water feature due to the continuum, and a relatively sharp 2.31-μm magnesium-hydroxl vibrational absorption with a weaker 2.4-μm feature. This spectrum is shown in Figure 3. Its composition was roughly 13-

17% Mg, 4-7% Fe, 3-6% Al, and 20-27% Si (see Figure 7). This composition is typical of smectite-group minerals.

A double-feature magnesium-iron phyllosilicate was also abundant, and seemed to fill vesicles. This phyllosilicate formed in unusual shapes, meaning it likely formed in cavities, directly from the aqueous fluid permeating through the rock rather than from alteration of olivine or pyroxene in-place. It was also a magnesium-iron phyllosilicate, with more abundant iron than the 2.31-μm feature saponite-like clay discussed above. This phyllosilicate was consistently bright in color and was not found in SR-425.

SR-425 and SR-459a had possible 2.31+2.38-μm alteration zones without a large 1.91-μm water band, but noise within the spectra was amplified due to low albedo. SEM composition mapping showed almost purely magnesium, silica, and oxygen. These could be serpentines or talc (King & Clark, 1989), but longer scanning time or more robust noise suppression methods are needed to verify the spectral characteristics and precisely identify the mineral.

Starting with SR-503, large hydration bands without any metal-hydroxl stretches began appearing, indicating zeolites. In SR-503, a more sodium rich matrix (3-4%) was present, and sodium and calcium rich zeolites were the primary alteration. There was no consistent zoning, though in a few cases a sodium rich core was surrounded by a sodium poor, slightly potassium and calcium enriched phase. These zeolites were all sharper featured, with analcime featuring a characteristic 1.8-μm absorption. The other species were very spectrally similar, but it was observed that Si/Al ratios were always less than four and cations were exclusively calcium, sodium, and potassium. This likely eliminates clinoptilolite as a possibility and makes a solution series of heulandite the most likely form of the non-analcime zeolites in SR-503. This zeolite

composition indicates temperatures of roughly 84-91° C during formation (Wohletz & Heiken, 1992). In addition to zeolites, pure-silica veinlets were found with SEM imaging in SR-503.

In 513b (4520 foot depth) zeolites are still the dominant alteration phase, but the magnesium rich saponite-like spectral endmember is also present in small abundances, seeming to replace primary minerals in the matrix. In 513b, a clear zoning of a potassium rich zeolite phase to the exterior of a sodium-calcium zeolite with broad features is present, as shown in Figure 3. The interior mixture matches a natrolite-scolecite mixture due to its exceptionally broad water bands and Na-Ca composition, while the exterior again matches a more aluminous, potassium dominated heulandite. Silica to aluminum ratios in all the zeolites are low, ranging from a little over 2 to close to 1 in some cases, eliminating several more silica rich zeolites with similar spectral features as possibilities.

SR-537b was dominated by the saponite-like phyllosilicates, but had small occurrences of a higher Si:Al zeolite matching a clinoptilolite or mordenite-like composition. Both slabs were also partially oxide-stained. While this makes them a candidate for extended surface aerial exposure, the alteration minerals are still characteristic of sub-aerial groundwater alteration. In these samples, the clay seemed more dispersed among the matrix due to a finer grained composition, similar to SR-503's matrix. Its composition and texture are nearly identical to the previous clays, with color ranging from dark green to black, as shown in the true color images in Figure 6.

SR-560's alteration mineralogy was composed entirely of the saponite-like material, which only differed by having a slightly lower aluminum concentration than in previous slabs. Its color was consistently a dull-green. The slab lacked zeolites and many of the clay occurrences were nearly perfectly spherical, suggesting vesicle infills. From these associations, it seems that

the saponite-ferrosaponite smectite forms both directly from alteration of olivine, and from solution of aqueous material. The morphologies can be observed in the true color images in Figure 6.

The final slab examined was SR-618 (5573 foot depth). Its alteration mineralogy was primarily composed of a fibrous, radiating zeolite which resulted in poor spectral data. However, zones where the water bands were expressed showed sharper bands, and the SEM indicated a high Si-Al ratio with 1% Ca and about 2% Na. This composition, combined with the very fibrous texture, makes it most likely mordenite. Mordenite forms under temperatures of 120-150 C ((Wohletz & Heiken, 1992) and is often associated with clinoptilolite, with which it may be mixed in this occurrence. Coatings of the saponite like clay were also present, though it was not pervasively replacing minerals. This can be observed in Figure 6.

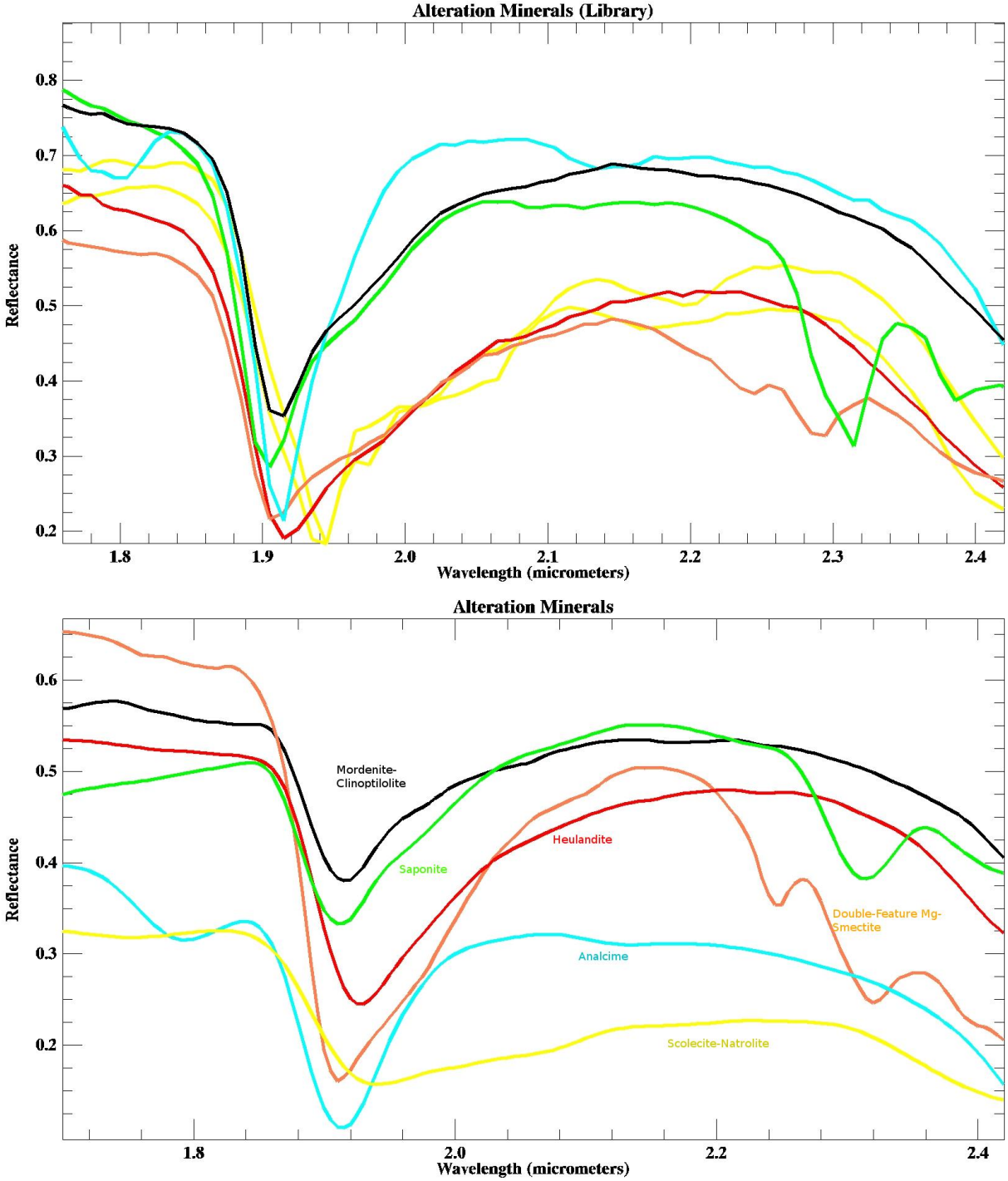

Figure 3: Alteration mineralogy compared to library minerals of similar species from Clark et al. (1993). The lower plot represent the average of all the mapped UCIS pixels shown with the same colors in the following figure, while the upper plots are library minerals. The two yellow spectra in the library mineral plot are scolecite and natrolite, showing the strong similarity between the two minerals. The coral colored spectrum is nontronite, another iron-mg smectite showing a similar double-feature to the smectite identified in 459a. The averaged spectrum of the double-feature smectite has its band centers shifted several nanometers from the nontronite spectrum, so the comparison is only for illustrative purposes.

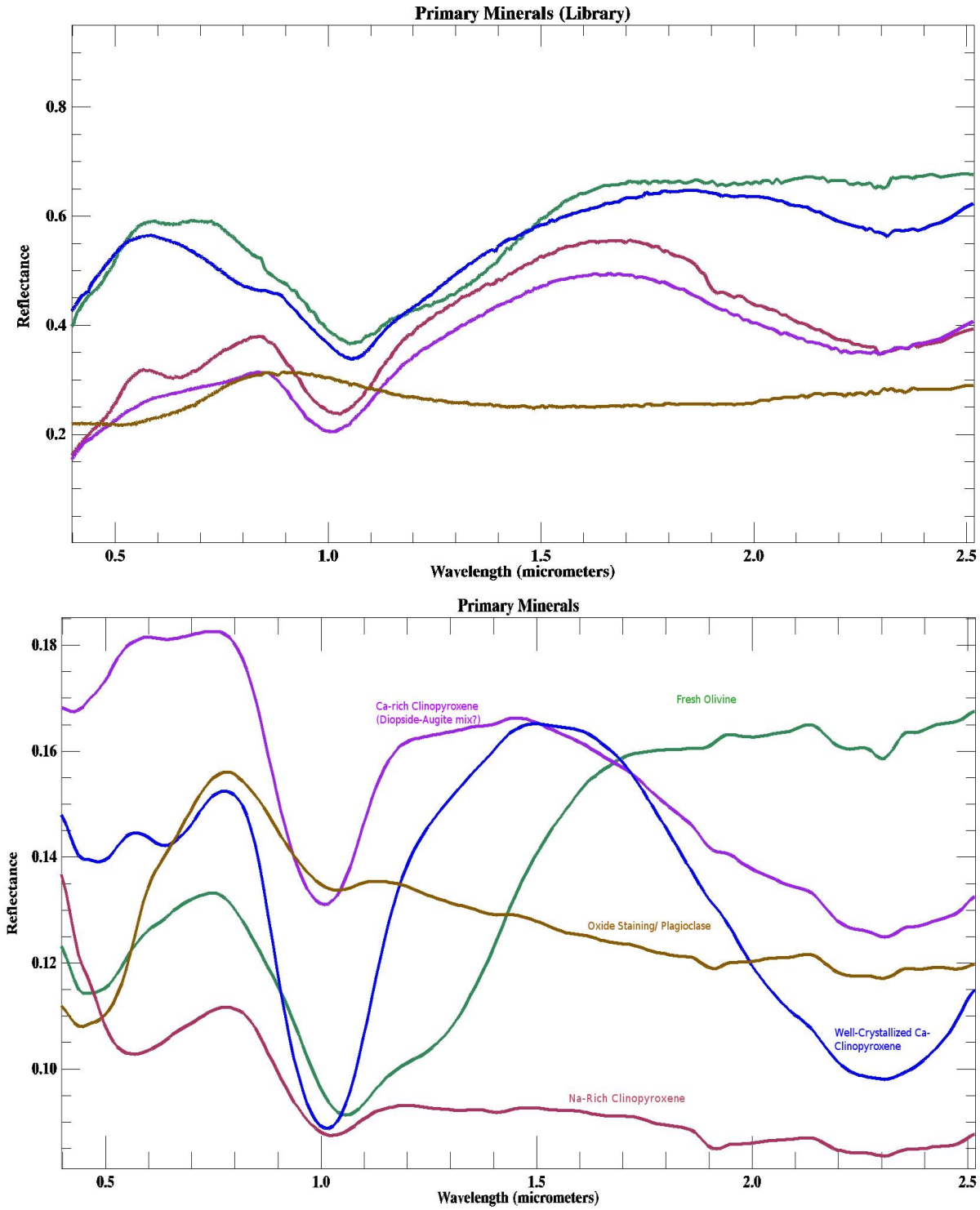

Figure 4: Primary mineralogy compared to library minerals of similar species from Clark et al. (1993). The lower plot represents the average of all the mapped UCIS pixels shown with the same colors in the following figures, while the upper plots are library minerals. The brown line in the library plot is a plagioclase feldspar, but when mixed with small amounts of iron/hematite the spectrum quickly approaches the UCIS average shown below. Notice in the fresh olivine averaged pixels, subtle features in the 2.2-2.4 micrometer range are present. These are possibly due to undifferentiated, higher noise pixels which could be serpentines or chlorites replacing olivine crystals.

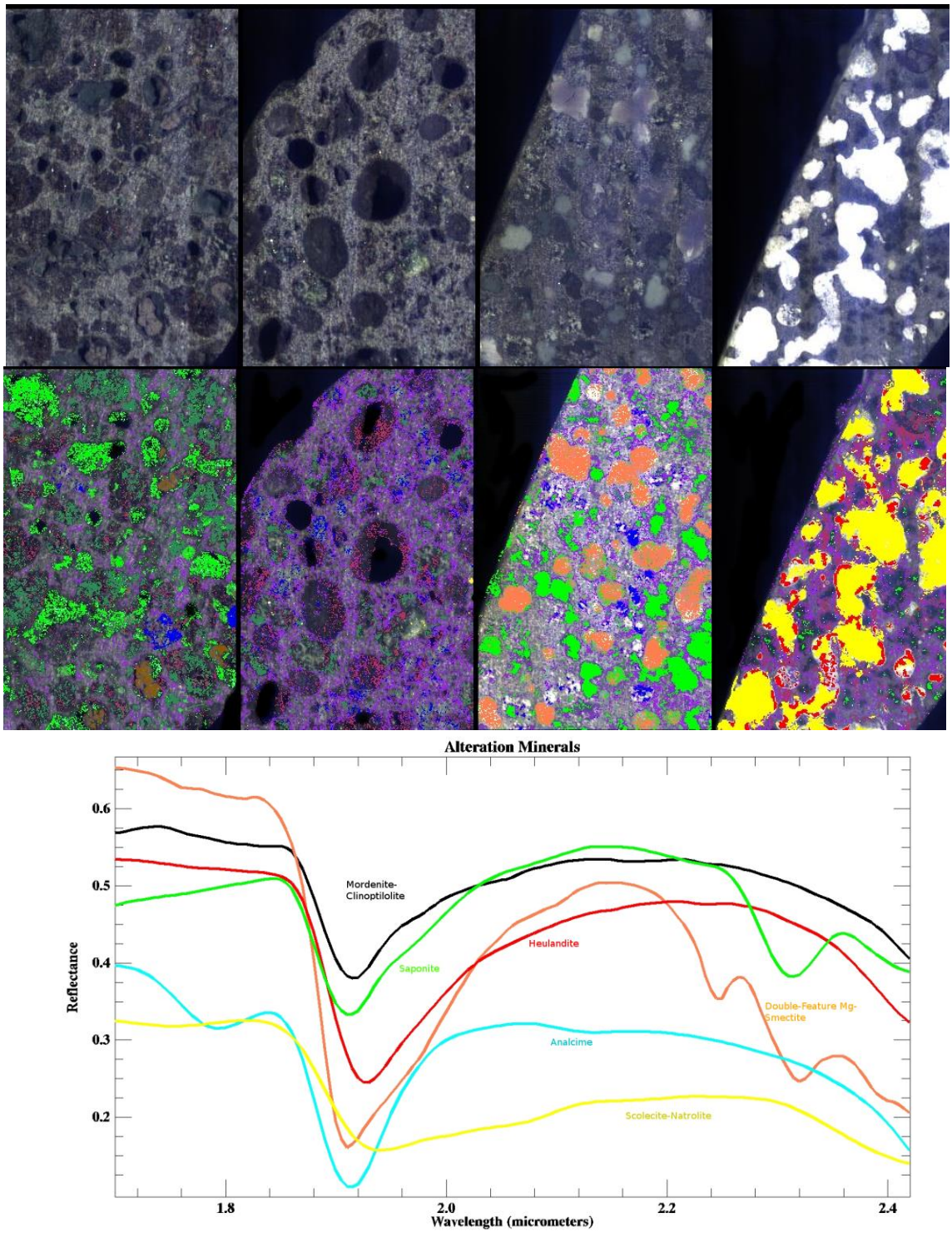

Figure 5: Mapped alteration mineralogy of (left to right): SR618,560,537b, and 503. Colors correspond to mapped minerals shown by spectra below, and follow the same color scheme as in Figures 3 and 4. In 618, fibrous mordenite-clinoptilolite fills voids coated in the saponite-ferrosaponite endmember. In 560, the saponite endmember pervasively fills vesicle-like voids, as well as replacing mafic minerals. In 537b, an oxide staining is present and matrix material markedly changes to a sodium rich, spectrally different pyroxene. Both saponite and scolecite-natrolite-like zeolites coexist. In 503, zeolites dominate and are mixed in composition and fill veins and veinlets. In both 503 and 537, the matrix appears broken up from post deposition stresses.

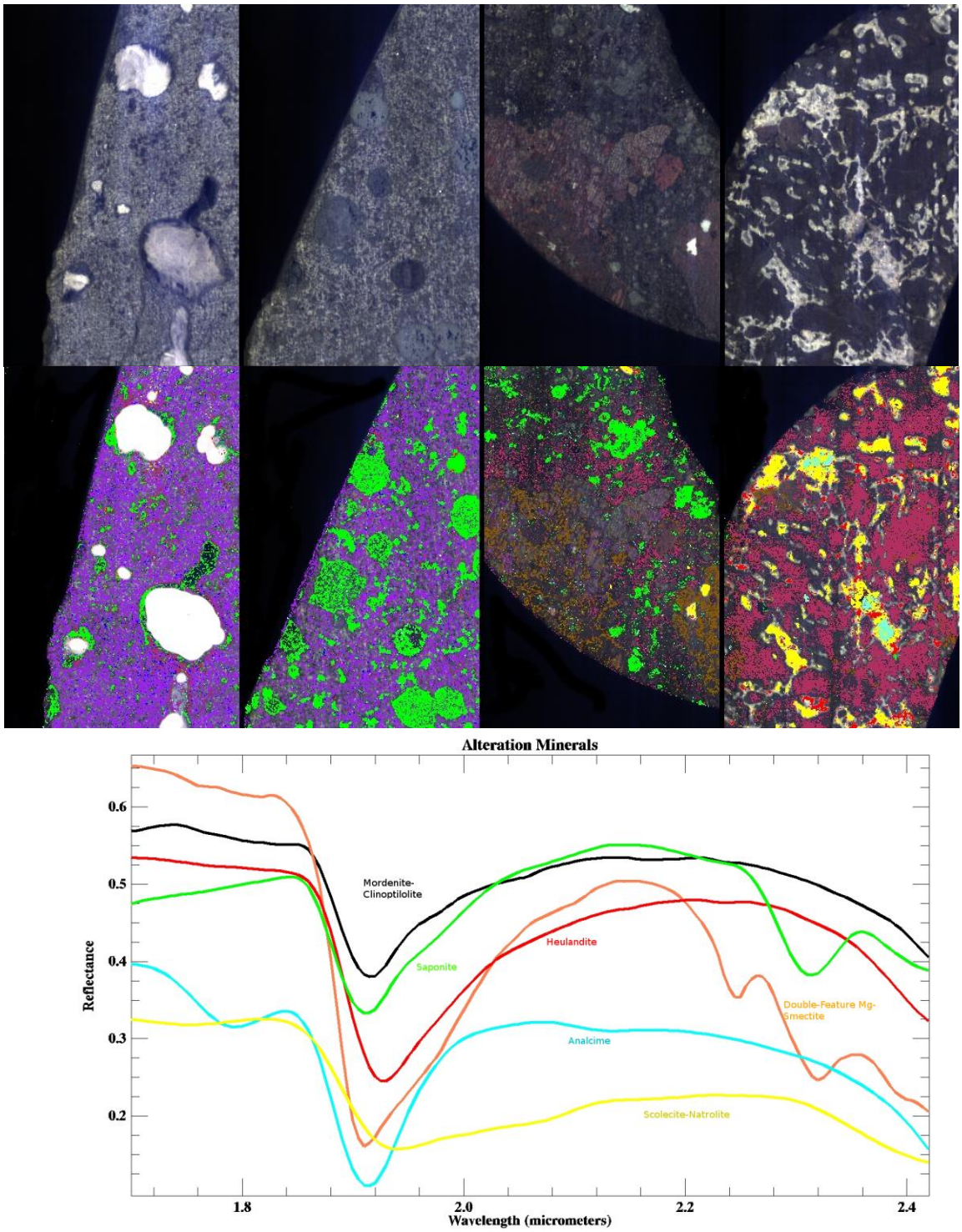

Figure 6: Mapped alteration mineralogy of (left to right): SR425, 392, 459a, 513b. Colors correspond to mapped minerals shown by spectra below and follow the same color scheme as Figures 3 and 4, though white mordenite-clinoptilolite in the image is plotted as black. In 425, fresh olivine can be seen closely spatially related to the saponite-like endmember. Here, the oxide stain endmember is falsely mapping plagioclase. In 392, no significant alteration is mapped, but hints of alteration around large crystals exist. In 459a, pervasive phyllosilicate alteration has replaced all large mafic crystals, with only sparse euhedral clinopyroxene left. The double-feature smectite fills strange shaped vesicle-like features. In 513b, zeolites dominate, but the potassium-rich heulandite endmember is seen forming rims around the broader-featured zeolites.

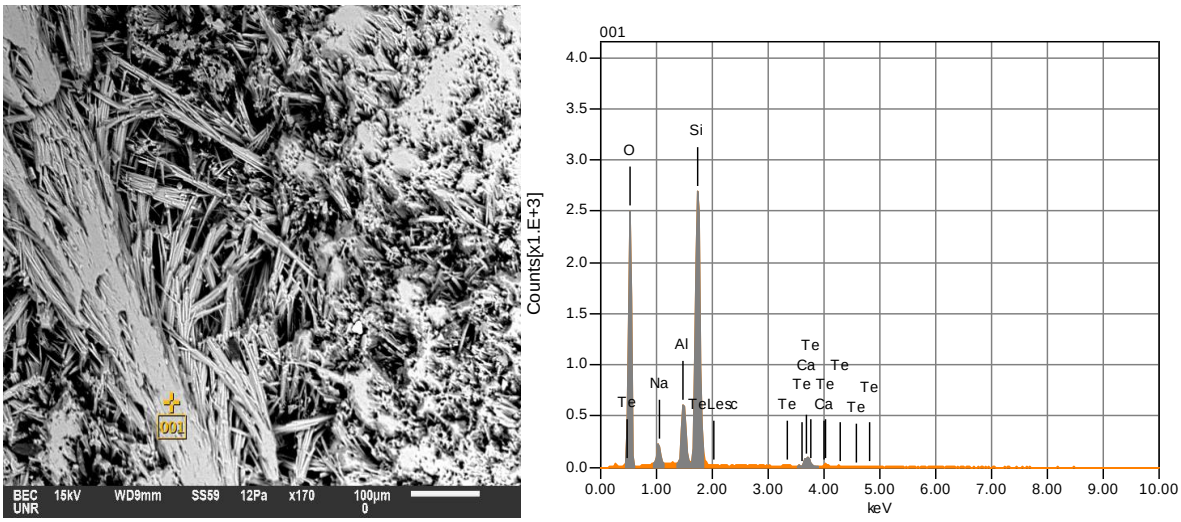

element	mass%	Atom%
O	53.70	67.52
Na	2.78	2.43
Al	6.48	4.83
Si	32.88	23.55
Ca	2.94	1.47
Total	100.00	100.00

Figure 7: Above is an image of the mordenite-clinoptilolite zeolite in SR-618, showing typical fibrous behavior. Its high Si:Al ratio, combined with the sodium and calcium abundances shown from the point EDS analysis to the left, narrow down its possible zeolite species substantially. The false Te ID's in the spectra are an example of the false readings given when performing EDS on imperfect topography. Below are EDS maps of 513b, showing a potassium rich zeolite replacing the scolecite-natrolite endmember.

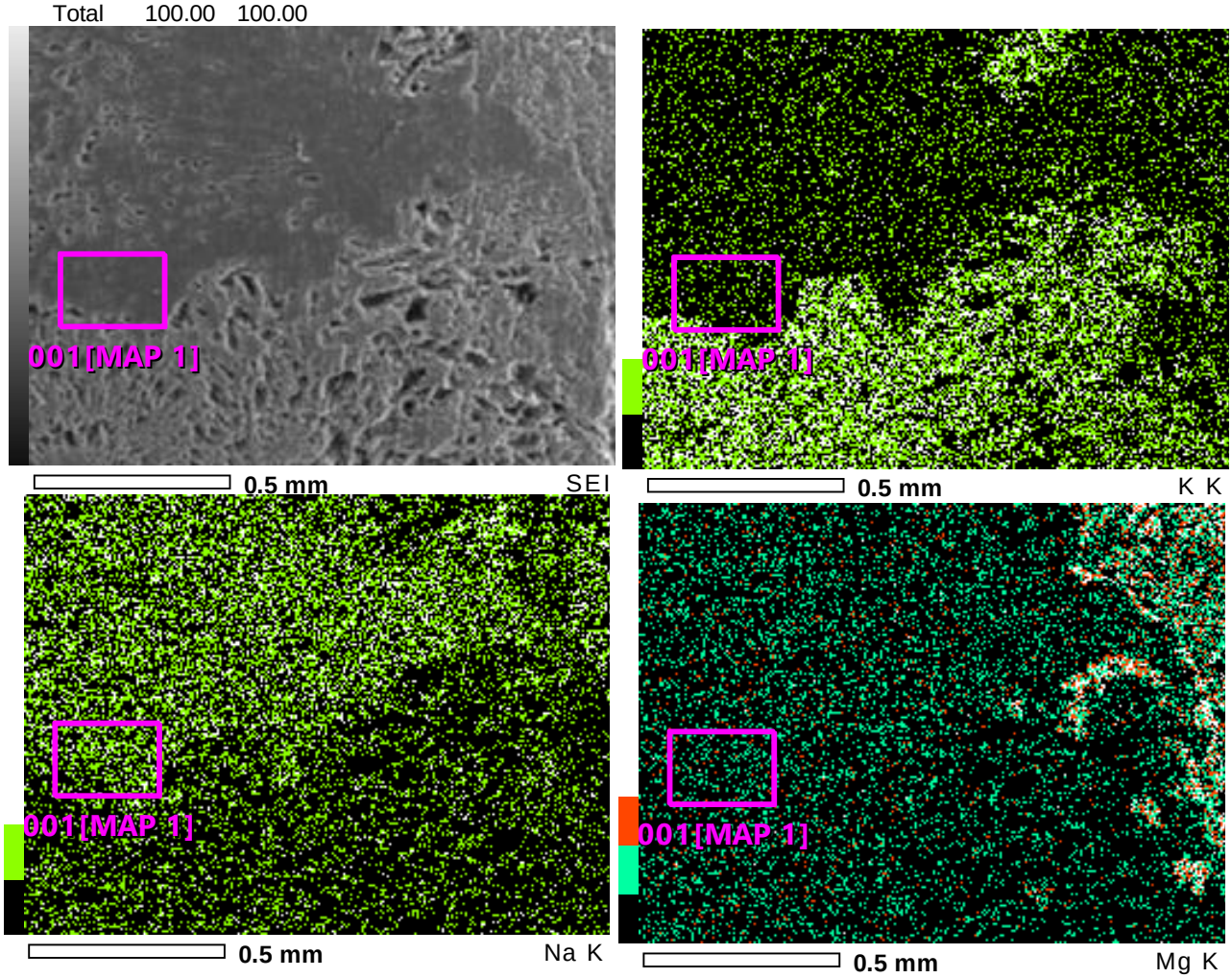

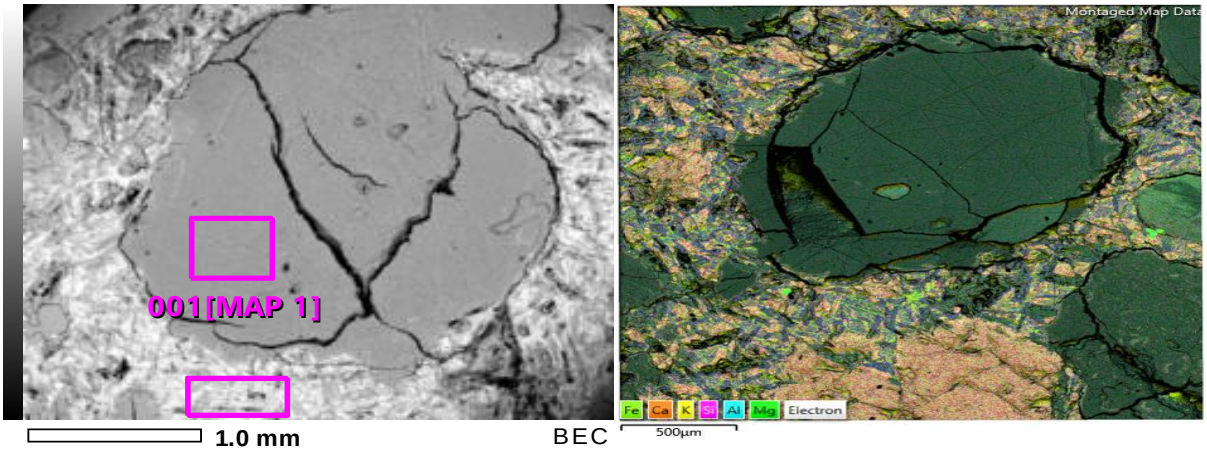

Figure 8: Above is the double-feature smectite in 459a. Here, the composition is referring to an average of the EDS spectra in the purple square. The high resolution 7100T map to the right shows calcic plagioclase distributed through the matrix. Below is a high magnification image of the same material, showing clay-like cleavage plating to the outside and a swelling texture characteristic of smectite clays towards the center of the infill.

element	mass%	Atom%
O	49.06	62.99
Mg	13.18	11.14
Al	8.41	6.40
Si	23.06	16.86
Ca*	2.03	1.04
Fe*	4.27	1.57
Total	100.00	100.00

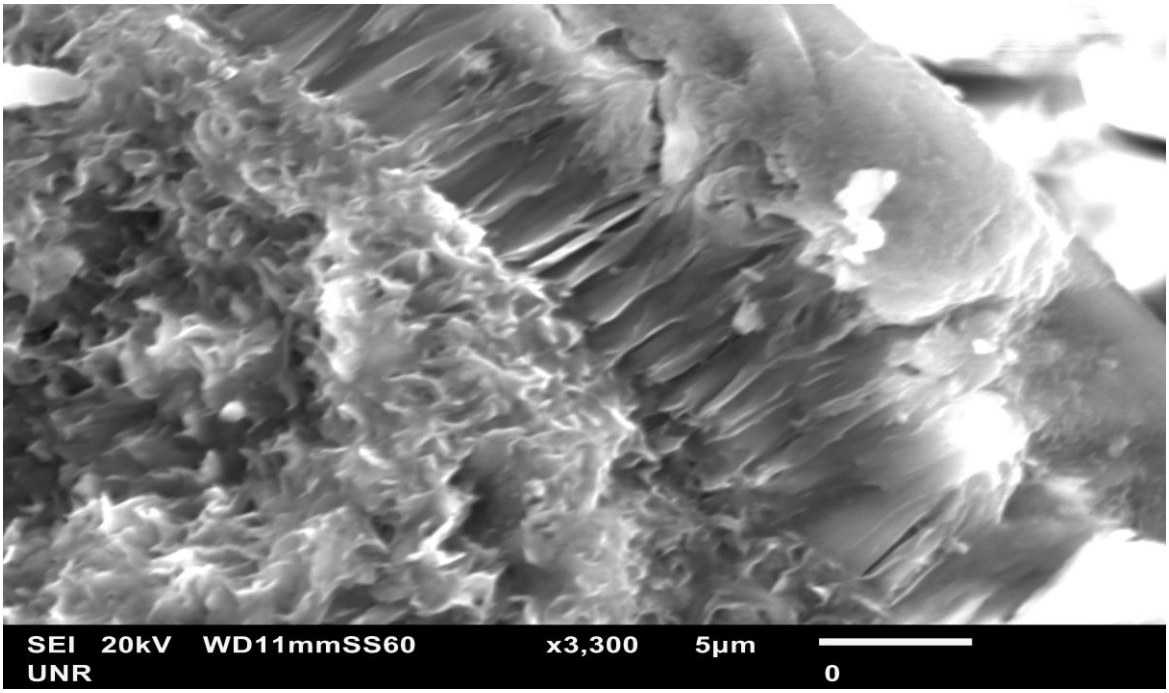

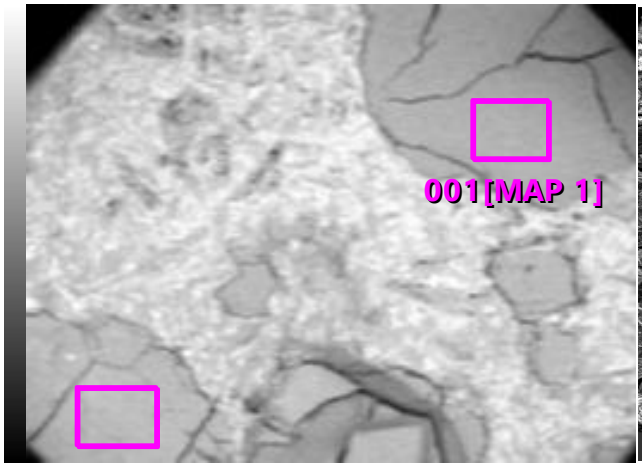

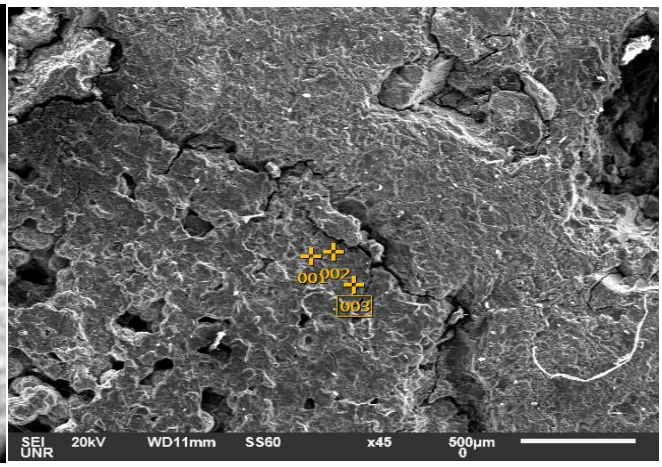

BEC

element	mass%	Atom%
O	52.06	63.51
Mg	13.45	11.29
Al	8.13	6.15
Si	22.86	16.61
Fe*	3.40	1.24
Total	100.00	100.00

	Fe	O	Mg	Al	Si
001	13.81	38.79	15.08	2.68	29.65
002	4.90	50.46	12.40	2.40	29.84
003	5.73	50.20	16.21	2.78	25.07
Average	8.15	46.48	14.56	2.62	28.19

Figure 9: Above is the saponite-like material from both 560 (right) and 459a (left). The EDS data is from averaged maps (purple squares) to the left and point spectra to the right. The texture here is different because the clay in 560 formed by precipitation, while the clay in 459a formed by replacement of olivine. Notice that the composition (mass %) is very similar, though these samples were collected hundreds of feet away from each other in depth. The 560 sample is slightly less aluminous and more iron rich.

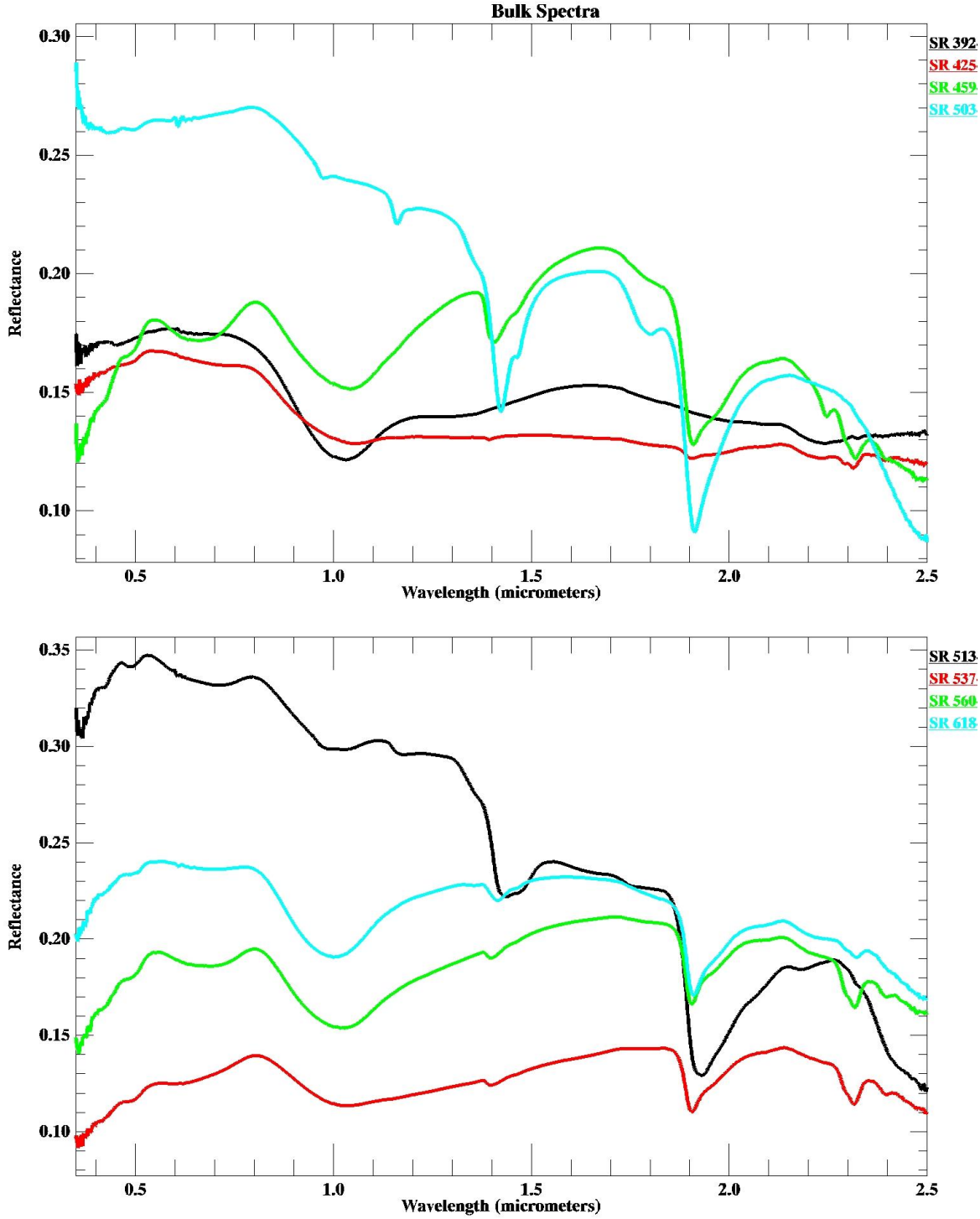

Figure 10: ASD collected bulk spectra of each cut-slab. Notice the many large water bands from pixels in SR-425 are nearly invisible in the bulk spectrum. Similarly, in SR-618, even relatively abundant mordenite-like zeolites produce rather weak water absorptions at 1.4 and 1.91 micrometers. The zeolite mixtures in SR-503 mask the abundant broader zeolites, while any signs of zeolite mixing in 513b are nearly invisible.

Alteration Mineralogy in Core:

Through a combination of linear unmixing and spectral feature fitting, best matches for single minerals were determined for all 781 ASD bulk spectra collected on the drill core. Linear unmixing was performed using averaged pixels from the UCIS imagery. Mixtures between zeolites and clays could be identified either by the presence of the 1.8-μm analcime band, or by disproportionately large 1.4-μm OH bands. In a few lines, a weak 2.21-μm Al-OH band was present, indicating an alteration mineral missing from the slabs. These lines might represent thin layers of surface alteration, or even ash layers or sedimentary deposits, all of which are present in very small amounts within the stratigraphy.

Zones of zeolite or phyllosilicate dominance were clear, with the 2.25-μm, 2.31-μm double feature phyllosilicate more abundant in thick layers higher in the stratigraphy, but persisted sparsely through the bottom of the hole. The 2.31-μm saponite-ferrosaponite clay was pervasive, and present in many of the spectra starting at about 3600 feet deep.

Zeolites commonly mix, as seen in the UCIS slabs, but broadening of the 1.91-μm water band as widely as in the scolecite-natrolite case, and the 1.8-μm analcime band can both only occur when the respective minerals are present. Unfortunately, the heulandite and mordenite type spectra are extremely difficult to distinguish from each other (though a band shift of about 2 nanometers was seen, see spectra above in Figure 3) and even more difficult in the presence of a pervasive clay with a similar 1.91-μm water band. Analcime was present in a few small zones higher in the hole, but was more abundant at depth. The broader water-absorption zeolites (scolecite-natrolite) were present at intermediate depths and towards the bottom of the hole as well. The heulandite type zeolites appeared to be at more intermediate depths, while mordenite-

clinoptilolite was present at intermediate depths through the bottom of the hole, though the mapping of these two zeolites is more uncertain.

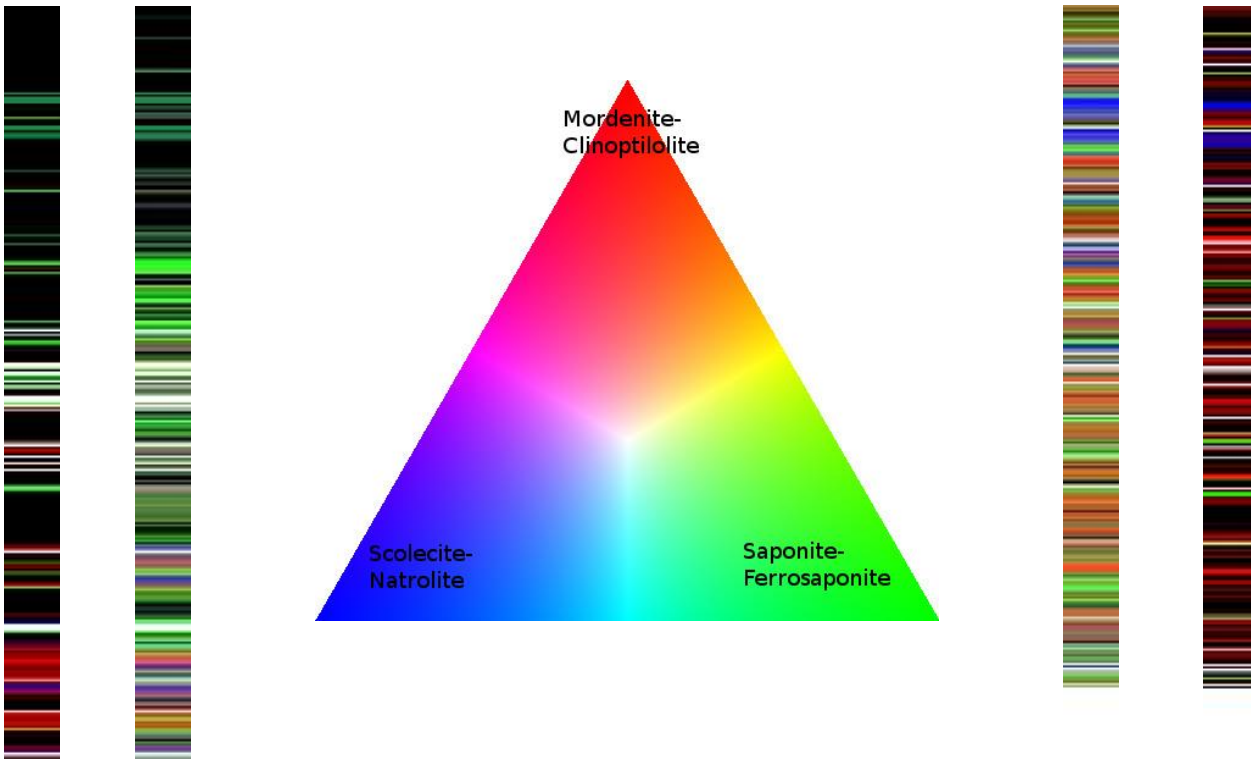

Figure 11: Mapped mineralogy of the core stack. The left two columns are roughly the top half of the scanned core (3,190-4600 feet depth) while the right two columns represent the bottom of the scanned section (4600-5785 ft). The images closer to the outside of the page are maps of best matches to single minerals, where the reds are sharper featured zeolites: mordenite, heulandite, and analcime (which has an orange tinge). White is the double featured phyllosilicate, bright green the saponite-like smectite, and blue the scolecite-natrolite zeolite. The two columns to the interior are three band composite images of spectral-feature fitting results, showing mixing of minerals through mixing of the three primary colors. Black represents a poor match to any single mineral, or a lack of alteration.

The ternary diagram above shows roughly what color certain mixtures of minerals will be in the composite images closest to the diagram. The only exceptions to this are the experience-based mapping of the double feature smectite, and fresh olivine, which are represented as sea green and white, respectively (the same as in the single-mineral match columns).

Overall, the correlation between the two outputs is good, but the utility of the mixed endmember image is clear. Areas of weak alteration are still represented and matched with endmembers, but are simply represented as more "washed out" colors. In addition, colors like the pinks and yellows show distinct mixtures instead of trying to fit only one mineral. The general trend of the hole is less-altered to more altered, with weaker phyllosilicate (425-like) alteration at the top, scolecite-natrolite-like zeolites with mixtures towards the center, and mordenite-heulandite-clinoptilolite zeolites towards the bottom. Phyllosilicate dominance seems to be more restricted deeper in the core, and might be tied to a lack of alkali cation availability in the aqueous fluid for zeolites to be prolific.

Discussion and Conclusions

Alteration History:

Nearly all of the collected samples clearly represent low temperature aqueous alteration from moderate to basic pH fluid. Bulk rock elemental composition stayed mostly constant, meaning hydrothermal brines or acidic sulfide leach material from overlying, younger volcanics likely did not affect these samples. Magnesium and iron rich phyllosilicates formed from olivine and pyroxenes in the country rock or precipitation from fluid and were not strongly stratigraphically controlled. Zeolites formed by replacing glass or precipitating from groundwater infused with alkali material.

Sulfates and carbonates are distinctly absent in the slabs and all bulk spectra. In addition, no underwater rapid-quenching textures such as pillow textures are present in the stratigraphy. These alone point to a lack of underwater extrusion of the basalts, as formation of dolomite and other carbonates, along with palagonite, would occur rapidly after extrusion. No biogenic textures were observed. The lack of heavy oxide formation, sulfates like jarosite, aluminous clays, and palagonite indicate that alteration occurred under the surface as well. If palagonite did form at the surface, it has likely been altered to the saponite-like clay (Sarkar et al., 2016).

The saponite-like clay seemed to form both in vesicles and in-place of primary olivine and ortho-pyroxene. It shared space with zeolites only when it formed in place of primary minerals. Zeolites dominated vesicle infills when the composition of the basalt matrix and primary mineralogy was more sodium rich, while the saponite-like material filled vesicles elsewhere, likely indicating more abundance of magnesium and iron in the aqueous fluid due to

faster dissolution of the primary minerals. It is likely that the vesicles infilled with saponite were once filled with zeolites but were replaced by saponite as the groundwater chemistry and depth changed (Sarkar et al., 2016).

The rimming of the zeolites with both other zeolites, and with the saponite-like clay was present at multiple depths. A reaction front could be seen in most cases from the SEM images, indicating a replacement process of one alteration mineral with another. The broader zeolites were generally being replaced by heulandite, mordenite, or clinoptilolite at depth. This is likely due to rising temperatures and pressures, rather than cation availability in the fluid. In the case of the deepest sample, SR-618, a saponite-like spectral signature was present surrounding the mordenite-like zeolite. This did not appear to be a replacement process, however, as there was no visible replacement in the SEM imagery and a coating of the saponite material was present in all of the visibly available vesicles. This indicates that both the mordenite-clinoptilolite and saponite were stable at this depth of 5573 feet.

No high-temperature geothermometer minerals were identified. Heulandite is generally a higher-temperature zeolite but can still form around 84° C. Mordenite can form and be stable from lower temperatures up to 230° C. Silica veining like that seen in 503 and 537a can occur at low and high temperatures (Wohletz & Heiken, 1992). Epidote, prehnite, and high temperature chlorites were absent. The low signal-noise ratio of dark minerals in the UCIS data might have limited identification, particularly of chlorites or serpentines which were suggested, but features were not interpreted with confidence in the noisy signals. However, the 2.34-μm feature of epidote, and the many distinct absorptions of prehnite were not seen in either the core or any UCIS slab.

Synergy Between SEM and Reflectance Spectroscopy:

The utility of correlated SEM composition analysis with reflection spectroscopy was demonstrated multiple times throughout this project. Without the initial spectroscopy to guide SEM examination, hundreds of hours could have been spent inspecting the eight slabs in order to be sure that the alteration mineral diversity had been adequately covered. Yet, without the aid of the SEM imaging and with only reflectance spectroscopy as a guide, the zeolite species likely would have been nearly impossible to delineate, and the phyllosilicates would have been difficult to identify due to the abundance of clays with a single 2.31-μm vibrational absorption. In addition, being able to identify cation composition of the primary mineralogy is useful.

In addition, the SEM allowed for inspection of features that even the 80 micrometer UCIS pixels could not identify. Thin veinlets of siliceous material in SR-503 (also found in SR-537a) are important observations and are not visible in the reflectance spectra. Textural observations, such as the swelling morphology of the 2.31-μm phyllosilicate, the fibrous nature of the mordenite, and the radiating nature of the other zeolites, are often invisible without great magnification.

Relevance to Mars Exploration and Future Work:

Ultimately, we used combinations of the UCIS image pixels to map the bulk spectra that were collected from the entire length of the altered section of the core. We used the higher spatial resolution data, where minerals are generally not mixed, to map specific alteration assemblages in the bulk spectra which were acquired with a spot size of ~ 2cm and always include multiple

minerals. Results presented here are promising and show that the constructed library is well representative of low-temperature groundwater alteration at neutral to basic pH in a Mars analog background lithology. This work has produced a spectral library which can be used as a starting point to map alteration assemblages on Mars from satellite or bulk rover spectroscopy, with reference to genetic source and possible depth/ P-T conditions at which the assemblage formed. It is significant that no high temperature or carbonate minerals were identified in this drill core, suggesting that locations where these minerals are observed on Mars would likely require different alteration conditions.

Further refinement of the phyllosilicate minerals represented in this project will require X-ray diffraction, and possibly transmission microscopy. While we have significantly narrowed the scope of possibilities, reflectance spectra of many minerals are inherently similar and the SEM used for compositional mapping does not provide true quantitative estimations of elemental abundances, only qualitative estimations. Once the spectral endmembers have been further narrowed to single minerals through further analytical methods, a core imaging scan could be performed. The endmembers identified in this study could then be used to map high resolution imaging spectra for the full length of the core, with a very high degree of certainty, and more complex relations could be understood. In addition, a core imaging scan could generate a near infinite number of synthetic mixes of spectra to produce bulk spectra of realistic alteration assemblages on Mars.

Another possibility is to use Mars analog dust coatings on the core to produce real spectra from the core that would more closely mimic spectra collected remotely from CRISM. This CRISM-like spectral library could then be used with methods such as SAM, linear unmixing, and spectral feature fitting to map alteration assemblages on Mars with minimal pre-processing.

These new methods of mapping alteration in CRISM data could lead to better mapping of exposed surface materials, streamlining the planning of costly rover traverse paths.

References

Alley, R.E. (1996). Algorithm Theoretical Basis Document for Decorrelation Stretch, *Jet Propulsion Laboratory, NASA*.

Bibring, J., Langevin, Y., Mustard, J., Poulet, F., Arvidson, R., Gendrin, A., . . . The OMEGA Team. (2006). Global mineralogical and aqueous Mars history derived from OMEGA/Mars Express data. *Science*, 312(5772). 400-404. http://www.jstor.org/stable/3845879

Blumers, M., Hamilton, J. C., Sanders, G. B., Zacny, K., Caillibot, E., Craft, J., . . . Sellar, R. G. (2013). Mauna Kea, Hawaii, as an analog site for future planetary resource exploration: Results from the 2010 ILSO-ISRU field-testing campaign. *Journal of Aerospace Engineering*, 26(1). 183-196. doi:10.1061/(ASCE)AS.1943 -5525.0000200

Calvin, W. M., & Pace, E. L. (2016). Mapping alteration in geothermal drill core using a field portable spectroradiometer. *Geothermics*, 61, 12-23. doi:10.1016/j.geothermics.2016.01.005

Clark, R. N., T. V. V. King, M. Klejwa, G. A. Swayze, & Vergo, N. (1990). High spectral resolution reflectance spectroscopy of minerals, *Journal of Geophysical Research: Solid Earth*, 95(B8), 12653–12680, doi:10.1029/JB095iB08p12653.

Clark, R.N., Swayze, G.A., Gallagher, A.J., King, T.V.V., and Calvin, W.M. (1993). The U.S. Geological Survey, Digital Spectral Library: Version 1 (0.2 to 0.3 μm). *U.S. Geological Survey Open-File Report* 93-592, 1326.

Ehlmann, B. L., Bish, D. L., Ruff, S. W., & Mustard, J. F. (2012). Mineralogy and chemistry of altered Icelandic basalts: Application to clay mineral detection and understanding

aqueous environments on Mars. *Journal of Geophysical Research: Planets, 117*(E11). doi:10.1029/2012JE004156

Ehlmann, B.L.., Mustard, J., & Murchie, S. (2010). Geologic setting of serpentine deposits on Mars. *Geophysical Research Letters, 37*(6). doi:10.1029/2010GL042596

Ehlmann, B. L., Mustard, J. F., Swayze, G. A., Clark, R. N., Bishop, J. L., Poulet, F., . . . Murchie, S. L. (2009).Identification of hydrated silicate minerals on Mars using MRO-CRISM: Geologic context near Nili Fossae and implications for aqueous alteration. *Journal of Geophysical Research - Planets,* 114, E00D08. doi:10.1029/2009JE003339

Gaskin, J. A., Jerman, G., Gregory, D., & Sampson, A. R. (2012). Miniature variable pressure scanning electron microscope for in-situ imaging & chemical analysis. *2012 IEEE Aerospace Conference Papers*.doi:10.1109/AERO.2012.6187064

Gotze, J., & Kempe, U. (2008). A comparison of optical microscope- and scanning electron microscope-based cathodoluminescence (CL) imaging and spectroscopy applied to geosciences. *Mineralogical Magazine, 72*(4). 909-924. doi:10.1180/minmag.2008.072.4.909

Graham, L. D., Morris, R. V., Graff, T. G., Yingst, R. A., ten Kate, I. L., Glavin, D. P., . . . Mumm, E. (2013). Moon and Mars analog mission activities for Mauna Kea 2012. *2013 IEEE Aerospace Conference Papers*. doi:10.1109/AERO.2013.6497195

King, T. V., & Clark, R. N. (1989). Spectral characteristics of chlorites and mg-serpentines using high-resolution reflectance spectroscopy. *Journal of Geophysical Research: Solid Earth,* 94(B10), 13997-14008. doi:10.1029/JB094iB10p13997

Kruse, F. A., Lefkoff,, A. B., Boardman, J. B. , Heidebrecht, K. B. , Shapiro, A. T., Barloon, P. J. &. Goetz A. F. H. (1993). The Spectral Image Processing System (SIPS) - Interactive Visualization and Analysis of Imaging spectrometer Data. *Remote Sensing of Environment*, 44, 145–163. doi:10.1016/0034-4257(93)90013-N

McCanta, M. C., Dyar, M. D., & Treiman, A. H. (2014). Alteration of Hawaiian basalts under sulfur-rich conditions: Applications to understanding surface-atmosphere interactions on Mars and Venus. *American Mineralogist, 99*(2), 291-302. doi:10.2138/am.2014.4584

Milliken, R. E., Swayze, G. A., Arvidson, R. E., Bishop, J. L., Clark, R. N., Ehlmann, B. L., . . . Weitz, C. (2008).Opaline silica in young deposits on Mars. *Geology, 36*(11), 847-850. doi:10.1130/G24967A.1

Ming, D. W., Morris, R. V., Bell, J. F., III, Graff, T. G., & Mertzman, S. A.(2003). Hydrothermal alteration on basaltic Mauna Kea volcano as a template for identification of hydrothermal alteration on basaltic mars. *Lunar and Planetary Science XXXIV Conference Papers.* https://www.sti.nasa.gov/sti-order-form/#.WESK2fkrK00

Pedersen, L. R., McLoughlin, N., Vullum, P. E., & Thorseth, I. H. (2015). Abiotic and candidate biotic micro-alteration textures in subseafloor basaltic glass: A high-resolution in-situ textural and geochemical investigation. *Chemical Geology, 410*, 124-137. doi:10.1016/j.chemgeo.2015.06.005

Ruffin, C., & King, R. L. (1999). The analysis of hyperspectral data using savitzky-golay filtering-theoretical basis. *IEEE 1999 International Geoscience and Remote Sensing Symposium*. 2(2), 756-758. doi:10.1109/IGARSS.1999.774430

Russ, J. C. (1984). Fundamentals of Energy Dispersive X-ray Analysis. *Butterworths. London.*

Sarkar, P.K., Devdutt, V.U., Vibhuti, W. (2016). Alteration of Volcanic Glass to Well-Crystallized Ferrosaponite in the Vesicles of the Deccan Trap Basalts at Bhuleshwar Ghat Section, Pune District, Maharashtra. *Journal of Geological Society of India,* 88, 22-28. doi:10.1007/s12594-016-0454-1

Shedd, K.B., Verta, R.L., & Wylie A.G. (1982) Size and shape characterization of fibrous zeolites by electron microscopy. *Report of Investigations (United States Bureau of Mines),* 8674. https://babel.hathitrust.org/cgi/pt?id=mdp.39015078490342;view=1up;seq=4

Tornabene, L. L., G. R. Osinski, A. S. McEwen, J. J. Wray, M. A. Craig, H. M. Sapers, and P. R. Christensen (2013). An impact origin for hydrated silicates on Mars: A synthesis. *Journal of Geophysical Research - Planets*, 118, 994–1012, doi:10.1002/jgre.20082.

Triana, J., Herrera, J., Rios, C., Castellanos, O., Henao, J., Williams, C., & Roberts, C. (2012). Natural zeolites filling amygdales and veins in basalts from the British tertiary igneous province on the Isle of Skye, Scotland. *Earth Sciences Research Journal, 16*(1), 41-53.

Ueda, H., Sawaki, Y., & Maruyama, S. (2016;2017). Reactions between olivine and CO2-rich seawater at 300 °C: Implications for H2 generation and CO2 sequestration on the early Earth. *Geoscience Frontiers,* 8*(*2), 387-396. doi:10.1016/j.gsf.2016.10.002

Wilson, S. A., A. D. Howard, J. M. Moore, and J. A. Grant (2016). A cold-wet middle-latitude environment on Mars during the Hesperian-Amazonian transition: Evidence from northern Arabia valleys and paleolakes, *Journal of Geophysical Research - Planets*, 121, 1667–1694, doi:10.1002/2016JE005052.

Wohletz, K., & Heiken, G. (1992). *Volcanology and Geothermal Energy. Berkeley, University of California Press*.

Wolfe, W., Wise, W., & Dalrympl, B. (1997). The Geology and Petrology of Mauna Kea Volcano, Hawaii: A Study of Postshield Volcanism. *United States Geological Survey Professional Paper 1557*. https://pubs.usgs.gov/pp/1557/report.pdf